# Anisotropic Electronic Structure and Perpendicular Magnetic Anisotropy in the Layered Ferromagnetic Semiconductor (Ba,K)(Zn,Mn)$_2$As$_2$ Elucidated by Angle-Dependent XMCD

The perpendicular magnetic anisotropy of the layered ferromagnetic semiconductor (Ba,K)(Zn,Mn)$_2$As$_2$ is studied by angle-dependent X-ray magnetic circular dichroism. We uncover the anisotropic distribution of Mn 3*d* electrons by extracting the magnetic dipole term. We find that the doped holes reside in the $d_{xz}$ and $d_{yz}$ orbitals, which are located higher in energy than the $d_{xy}$ orbital because of the $D_{2d}$ splitting that arises from the distorted MnAs$_4$ tetrahedra. We find that the perpendicular magnetic anisotropy originates from the degeneracy lifting of *p*-$d_{xz}$, $d_{yz}$ hybridized states at the Fermi level when spins are aligned along the *z*-axis direction.

Ferromagnetic semiconductors (FMSs) have been studied intensively as they are attractive for future applications. $(Ba_{1-x}K_x)(Zn_{1-y}Mn_y)_2As_2$ is a recently found FMS [1] and has a layered crystal structure, as shown in Fig. 1(a). Unlike prototypical FMSs such as (Ga,Mn)As, the number of carriers and spins can be controlled by the heterovalent $K^+$-$Ba^{2+}$ substitution and the isovalent $Mn^{2+}$-$Zn^{2+}$ substitution, respectively. The ferromagnetism has been reported to be carrier-induced, and the Curie temperature ($T_C$) reaches 230 K, exceeding the $T_C$ of (Ga,Mn)As, 200 K. Since the crystal structure is anisotropic, having distorted MnAs$_4$ tetrahedra, sizeable perpendicular magnetic anisotropy (PMA) emerges in this system [2].

In this work, we reveal how the anisotropic crystal structure gives rise to the PMA in (Ba,K)(Zn,Mn)$_2$As$_2$ by performing angle-dependent X-ray absorption spectroscopy (XAS) and X-ray magnetic circular dichroism (AD-XMCD) measurements. In conventional XMCD measurement systems, magnetic fields are fixed parallel to the X-rays [longitudinal geometry, Fig. 1(b)], and spin magnetic moments ($M_S$) are predominantly probed. In this study, on the other hand, we applied magnetic fields such that the spin magnetic moment became perpendicular to the X-rays [transverse geometry, Fig. 1(c)]. In this way, we can extract the magnetic dipole term ($M_T$), a hallmark of the anisotropic spin distribution [3].

We measured $Ba_{0.904}K_{0.096}(Zn_{0.805}Mn_{0.195})_2As_2$ single crystals with $T_C$ = 60 K. Figure 1(d) shows the XAS and XMCD spectra taken in the longitudinal geometry (LXMCD). Figure 2(a) shows the XMCD spectra taken in the transverse geometry (TXMCD). The distinct TXMCD spectra guarantee that the TXMCD signals do not originate from a residual spin component but from the magnetic-dipole-term component, highlighting the anisotropic Mn 3*d* spin distribution in (Ba,K)(Zn,Mn)$_2$As$_2$.

In order to understand the LXMCD and TXMCD spectra, we performed configuration-interaction cluster model calculations, the results of which are shown in Figs. 1(d) and 2(a). Here, the used parameters are the same as those used for (Ga,Mn)As [4] except for the $D_{2d}$ splitting that accounts for the distorted MnAs$_4$ tetrahedra. Note that the LXMCD spectra can be reproduced regardless of the $D_{2d}$ splitting, but the TXMCD spectra require the $D_{2d}$ splitting. The calculation indicates that the $d_{xz}$ and $d_{yz}$ states should be located higher in energy than the $d_{xy}$ states and that the $d_{x^2-y^2}$ state should be located higher than the $d_{z^2}$ state.

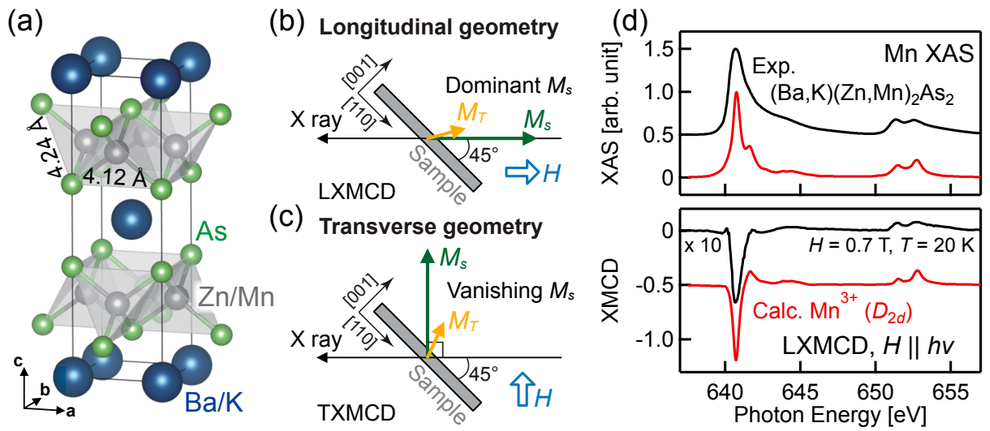


Figure 1: (a) Crystal structure. (b) and (c) XMCD measurement geometries. (d) Mn $L_{23}$-edge XAS and XMCD spectra taken in the longitudinal geometry (LXMCD). The calculated spectra are also shown by the red curves.

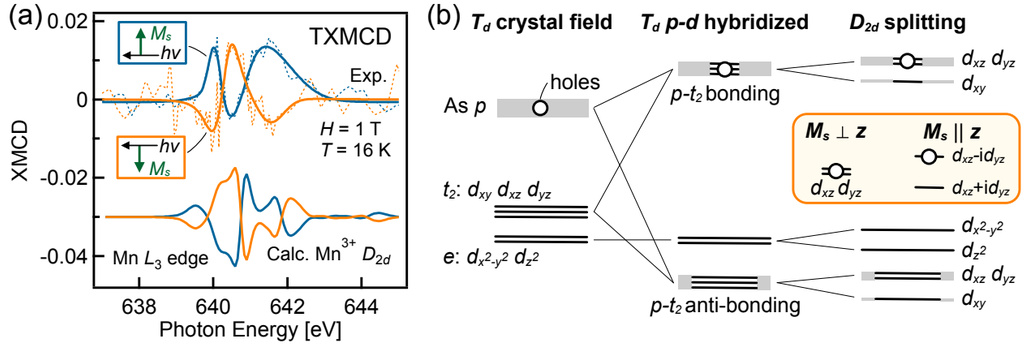


Figure 2: (a) Mn $L_3$-edge XMCD spectra taken in the transverse geometry (TXMCD). (b) Schematic energy diagram of the occupied majority-spin Mn 3*d* orbitals in (Ba,K)(Zn,Mn)$_2$As$_2$. White circles represent doped holes. Inset shows how the top-most $d_{xz}$ and $d_{yz}$ levels with holes result in energy gain depending on the spin orientation.

Figure 2(b) schematically summarizes the present findings. Under the tetrahedral crystal field, the Mn 3*d* orbitals are split into doubly generate e ($d_{x2-y2}$, $d_{z2}$) orbitals and triply degenerate $t_2$ ($d_{xy}$, $d_{yz}$, $d_{zx}$) orbitals, as shown in the left column of Fig. 2(b). The $t_2$ orbitals hybridize with the As 4*p* orbitals and form bonding and antibonding *p*-$t_2$ orbitals, while the *e* orbitals remain intact, as shown in the middle column. This configuration is realized in cubic (Ga,Mn)As, and holes residing in the antibonding *p*-$t_2$ orbitals mediate the ferromagnetic interaction. In the case of (Ba,K)(Zn,Mn)$_2$As$_2$, the elongation of the MnAs$_4$ tetrahedra further splits $t_2$ levels into $d_{xz,yz}$ and $d_{xy}$ levels and *e* levels into $d_{x2-y2}$ and $d_{z2}$ levels, as shown in the right column of Fig. 2(b). The doped holes thus reside in the *p*-$d_{xz,yz}$ hybridized orbitals.

Magnetocrystalline anisotropy results from the energy gain through spin-orbit coupling when spins are aligned along a specific direction, and only the orbitals near the Fermi level are relevant. In the present system, *p*-$d_{xz,yz}$ hybridized orbitals with holes are responsible for the PMA. The inset of Fig. 2(b) illustrates how the PMA appears in (Ba,K)(Zn,Mn)$_2$As$_2$. When spins are aligned along the *z*-axis, the degeneracy of $d_{xz,yz}$ will be lifted due to spin-orbit interaction to form $d_{xz} \pm id_{yz}$ orbitals, resulting in an energy gain. On the other hand, when spins are aligned in the x-y plane, the $d_{xz,yz}$ orbitals remain degenerate, and therefore there is no energy gain.

To summarize, the PMA originates from the energy gain due to the degeneracy lifting of *p*-$d_{xz,yz}$ orbitals at the Fermi level when spins are aligned along the *z*-axis. The present results [5] also suggest that it is possible to control the magnetic anisotropy by engineering the magnitude of the $D_{2d}$ splitting; this new degree of freedom would be helpful in future applications.

## REFERENCES

[1] K. Zhao, Z. Deng, X. C. Wang, W. Han, J. L. Zhu, X. Li, Q. Q. Liu, R. C. Yu, T. Goko, B. Frandsen, L. Liu, F. Ning, Y. J. Uemura, H. Dabkowska, G. Luke, H. Luetkens, E. Morenzoni, S. R. Dunsiger, A. Senyshyn, P. Böni and C. Q. Jin, *Nat. Commun.* **4**, 1442 (2013).

[2] G. Q. Zhao, C. J. Lin, Z. Deng, G. X. Gu, S. Yu, X. C. Wang, Z. Z. Gong, Y. J. Uemera, Y. Q. Li and C. Q. Jin, *Sci. Rep.* **7**, 14473 (2017).

[3] G. Shibata, M. Kitamura, M. Minohara, K. Yoshimatsu, T. Kadono, K. Ishigami, T. Harano, Y. Takahashi, S. Sakamoto, Y. Nonaka, I. Keisuke, Z. Chi, M. Furuse, S. Fuchino, M. Okano, J. Fujihira, A. Uchida, K. Watanabe, H. Fujihira, S. Fujihira, A. Tanaka, H. Kumigashira, T. Koide and A. Fujimori, *npj Quantum Mater.* **3**, 3 (2018).

[4] M. Kobayashi, H. Niwa, Y. Takeda, A. Fujimori, Y. Senba, H. Ohashi, A. Tanaka, S. Ohya, P. N. Hai, M. Tanaka, Y. Harada and M. Oshima, *Phys. Rev. Lett.* **112**, 107203 (2014).

[5] S. Sakamoto, G. Q. Zhao, G. Shibata, Z. Deng, K. Zhao, X. Wang, Y. Nonaka, K. Ikeda, Z. Chi, Y. Wan, M. Suzuki, T. Koide, A. Tanaka, S. Maekawa, Y. J. Uemura, C. Q. Jin and A. Fujimori, *ACS Appl. Electron. Mater.* **3**, 789 (2021).

## BEAMLINE

BL-16A2

**S. Sakamoto[1], G. Q. Zhao[2], G. Shibata[1], Z. Deng[2], K. Zhao[2], X. C. Wang[2], Y. Nonaka[1], K. Ikeda[1], Z. Chi[1], Y. Wan[1], M. Suzuki[1], T. Koide[3], A. Tanaka[4], S. Maekawa[5, 6], Y. J. Uemura[7], C. Q. Jin[2] and A. Fujimori[1, 8] ([1]The Univ. of Tokyo, [2]Chinese Academy of Sciences, [3]KEK-IMSS-PF, [4]Hiroshima Univ., [5]RIKEN, [6]Univ. of Chinese Academy of Sciences, [7]Columbia Univ., [8]Waseda Univ.)**